

*Proceedings of IACS*

---





## Orbital ice and its melting phenomenon\*

Tapan Chatterji

Institut Laue-Langevin, BP 156, 38042 Grenoble Cedex 9, France

E-mail : chatt@ill.fr

**Abstract** : We coin a phrase “orbital ice” to describe the orbitally ordered phase of  $\text{LaMnO}_3$ , which is formed by the cooperative Jahn-Teller transition below  $T_{JT} \approx 750$  K. We interpret the transition at  $T_{JT}$  to be a “melting” of the “orbital ice” by analogy with the phenomenon of ice melting. We will demonstrate some similarities between the two melting phenomena of which the first phenomenon is of electronic origin and the other of course is a well known lattice melting known to humanity for hundreds of centuries.

**Keywords** : Orbital ordering, Jahn-Teller transition, X-ray diffraction, neutron diffraction

**PACS Nos.** : 61.12.Ld, 61.66.Fn

Chemists have been fond of talking about orbitals and drawing them on paper and on black boards during discussions and lectures ever since quantum mechanics was used successfully to explain bonding in molecules and solids. Thus, quantum chemistry was about orbitals and orbitals became the bread and butter of intuitive chemists. The solid state physicists talked less about orbitals and more and more about the bands and electronic structure of the entire solid until recently. For a long time, condensed matter physicists discussed about metals and semiconductors and the wonderful properties of atoms when they come together to form a solid. Then came the revolution! Bednorz and Müller discovered superconductivity [1] in the perovskite  $\text{La}_{2-x}\text{Ba}_x\text{CuO}_4$  below  $T_c \approx 35$  K. Condensed matter physicists all over the world worked frantically and explored layer perovskite cuprates and other related materials and found superconductivity below  $T_c \approx 145$  K. The physicists had to master all the techniques of solid state chemistry, synthesis included. They learned the age old ceramics techniques. They started growing single crystals by the flux method and also by the zone melting technique which they had learned already during the hay days of semiconductor technology. Theoretical condensed matter physicists worked day and night to master mathematical techniques used in different branches of physics and employed them to solve the mystery of superconductivity

in layered perovskite cuprates. They were soon humbled of course! However, the intuitive approach of the solid state chemists somehow diffused through the minds of experimental condensed matter physicists. They often talked about  $d$  orbitals of Cu and even drew them on paper and blackboards as chemists have been doing for decades. Armed with the experience gained during the research in superconducting cuprate materials, condensed matter physicists turned their interest to another class of transition metal oxides, the perovskite manganites. The manganites had been already investigated in the nineteen fifties[2-7]. Now condensed matter physicists suddenly rediscovered them [8–18]. Their strong negative magnetoresistive properties were already known. However, this time the condensed matter physicists were able to magnify this effect by choosing the right materials, and called it colossal magnetoresistance (CMR). Hundreds of scientific papers were written overnight! Many of them used the expressions “orbital”, “orbital degrees of freedom” and some simply talked about “orbital physics”. Suddenly, orbitals became fashionable. Y. Tokura and N. Nagaosa[14], the two most very prominent players in the game of orbital physics wrote in their review article in Science:

“An electron in a solid, that is, bound to or nearly localised on the specific atomic site, has three attributes: charge, spin and orbital. The orbital represents the shape of the electron cloud in a solid. In transition-metal oxides with anisotropic-shaped  $d$ -orbital electrons, the Coulomb interaction between the electron

\* A part of the Ripon Professorship Endowment Lecture delivered on February 6, 2006 at the Indian Association for the Cultivation of Science, Jadavpur, Kolkata, India.

(strong electron correlation effect) is of importance for understanding their metal- insulator transitions and properties such as high-temperature superconductivity and colossal magnetoresistance. The orbital degrees of freedom occasionally play an important role in these phenomena through strong coupling with charge, spin and lattice dynamics. An overview is given on this “orbital physics”, which will be a key concept for the science and technology of correlated electrons.”

Let us now examine what “orbitals” are and check what is so fascinating about them. The name “orbital” originated from the electron orbits of the old quantum theory where electrons were imagined to have something like planetary orbits of the classical Newtonian mechanics. The name “orbitals” still persisted in the new quantum mechanics where electron orbits had no meaning whatsoever. Thus, “orbitals” were retained in the literature when the Schrödinger wave equation was used to determine the energy levels of the hydrogen atom. In 1926, Schrödinger proposed the wave equation which now bears his name. The derivation of the wave equation was based on two most important earlier contributions. First, Louis de Broglie suggested a dual wave-particle nature of electrons, which was confirmed by the diffraction of electrons by a crystal. Secondly, Heisenberg stated his uncertainty principle which dictates that the position and the momentum of a particle cannot be simultaneously precisely determined. The wave functions are the solutions of the Schrödinger wave equation given by

$$\frac{\partial^2 \Psi}{\partial x^2} + \frac{\partial^2 \Psi}{\partial y^2} + \frac{\partial^2 \Psi}{\partial z^2} + \frac{8\pi^2 m}{h^2} (E - V) \Psi = 0, \quad (1)$$

where  $\Psi$  is the wave function,  $x, y, z$  are the coordinates in space,  $m$  is the mass,  $h$  is the Planck's constant,  $E$  is the total energy and  $V$  is the potential energy. This equation describes the behaviour of subatomic particles much as the macroscopic particles are described by the classical mechanics. It is found that the solution for the hydrogen atom contains three quantum numbers  $n, l$  and  $m_l$ . Each solution found for a different set of  $n, l$  and  $m_l$  is called an eigenfunction and represents an orbital of the hydrogen atom. One would require a four dimensional graph to plot the complete wave function. It is customary therefore to split the wave function  $\Psi$  into three parts as

$$\Psi_{nlm}(r, \theta, \phi) = R_{nl}(r) \cdot \Theta_{lm}(\theta) \cdot \Phi_m(\phi), \quad (2)$$

where  $R(r)$  gives the radial dependence of the wave function whereas  $\Theta(\theta)$  and  $\Phi(\phi)$  give the angular dependence. The angular part of the wave function determines the shape of the electron cloud and is dependent on the type of orbital involved ( $s, p, d$  or  $f$ ) and its orientation in space. But for a given type of orbital such as  $s$  or  $p_z$ , the angular part of the wave function is independent of the principal quantum number  $n$  or the energy level. Sometimes, instead of plotting the angular part of the

wave functions, we would like to plot the function  $\Theta^2 \Phi^2$  which corresponds to the angular part of  $\Psi^2$  and hence gives the probability of finding an electron. The squared orbitals look very similar to the original orbitals:  $s$  orbitals are still spherical but the lobes  $p, d \dots$  look only more flattened. The sign of the original wave function is sometimes still retained on the plots of the squared orbitals. This is useful for bonding considerations where the sign of the wave function is very important. Figure 1 shows some of the hydrogen-like orbitals. For further details about atomic orbitals, the reader is advised to consult the standard text books on atomic physics and quantum chemistry [19,20].

In the physics of manganites, two types of orbitals are important, namely, the  $3d$  orbitals of Mn and the  $2p$  orbitals of O atoms. The Mn ion in  $\text{LaMnO}_3$  is surrounded by the six O atoms forming approximately an octahedron. The five-fold degenerate  $3d$  orbitals  $d_{xy}, d_{yz}, d_{zx}, d_{x^2-y^2}$  and  $d_{3z^2-r^2}$  are split into two groups of  $t_{2g}$  and  $e_g$  representations of the cubic group  $O_h$  in an octahedral crystal field. The lower-lying  $t_{2g}$  orbitals are  $d_{xy}, d_{yz}$  and  $d_{zx}$  whereas the higher-lying  $e_g$  orbitals are  $d_{x^2-y^2}$  and  $d_{3z^2-r^2}$ . In undistorted octahedral field, the  $t_{2g}$  orbitals are triply degenerate while the  $e_g$  orbitals are doubly degenerate, but the degeneracy is removed by the Jahn-Teller [21] distortion. In the CMR perovskite materials, the electron-electron interactions are such that other configurations of the  $t_{2g}$  levels involving a different number of electrons or not all spins parallel are much higher in energy so that  $t_{2g}$  levels with three parallel spins constitute a “core-spins” of magnitude  $S = 3/2$ . The conventional choice of the basis set for the  $e_g$  level is  $|3z^2 - r^2\rangle$  and  $|x^2 - y^2\rangle$ . The  $|3z^2 - r^2\rangle$  wavefunction is elongated in the  $z$  direction, but has smaller extent in the  $x$ - $y$  plane. The  $|x^2 - y^2\rangle$

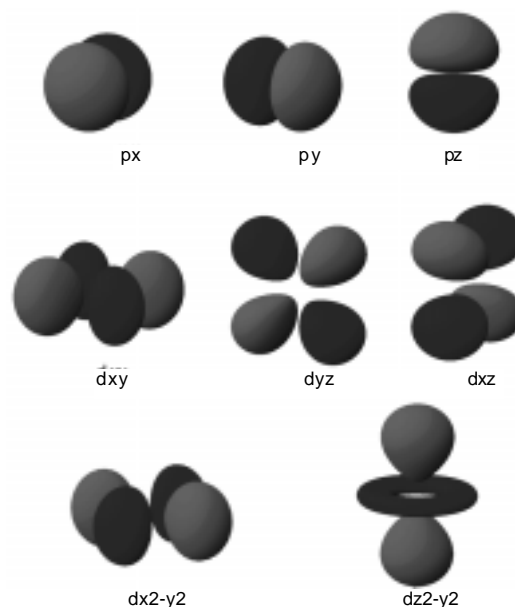


**Figure 1.** Schematic representation of  $p$  and  $d$  atomic orbitals. The signs of the wave functions are represented by the grey and black colours.

wavefunction is spread out in the  $x$ - $y$  plane and has small extent in the  $z$ -direction. The  $|x^2 - y^2\rangle$  changes sign under  $\pi/2$  rotation about the  $z$  axis, but  $|3z^2 - r^2\rangle$  wavefunction does not. One may obtain wavefunctions with principal axes in any direction by choosing appropriate linear combinations:

$$|3x^2 - r^2\rangle = \frac{\sqrt{3}}{2}|x^2 - y^2\rangle + \frac{1}{2}|3z^2 - r^2\rangle, \quad (3)$$

$$|3y^2 - r^2\rangle = \frac{\sqrt{3}}{2}|x^2 - y^2\rangle - \frac{1}{2}|3z^2 - r^2\rangle.$$

The Mn atoms in a perovskite structure are too far apart for direct overlap and any electron hopping must go *via* virtual states on the intermediate O atoms. The important intermediate states are the O  $2p$  orbitals of which the most important is the  $O_{2p\sigma}$  which extends from the O towards the neighbouring Mn. This orbital has a strong overlap with the  $|3z^2 - r^2\rangle$ , but is orthogonal to the  $|x^2 - y^2\rangle$  in the ideal perovskite structure. The other O  $2p$  orbital, namely, the  $O_{2p\pi}$  is orthogonal to both  $|3z^2 - r^2\rangle$  and  $|x^2 - y^2\rangle$  orbitals in the ideal cubic perovskite structure. The deviation of the ideal perovskite structure will allow some overlap of  $|x^2 - y^2\rangle$  with the  $O_{2p\sigma}$  and  $O_{2p\pi}$  orbitals.

It has now become increasingly clear that the physics of strongly correlated transition metal oxides is largely influenced by the orbital degrees of freedom in addition to the usual charge, spin and lattice degrees of freedom. The orbital degrees of freedom becomes specially important in the case of the transition metal oxides with orbital degeneracy that exists for an undistorted octahedral coordination, for example in a regular  $MnO_6$  octahedron. In an isolated  $MnO_6$  octahedron, this gives rise to the Jahn-Teller effect [21, 22] mentioned earlier. In a concentrated system in the solid state, the degeneracy gives rise to a cooperative Jahn-Teller transition and an orbital ordering transition along with a structural transition. The undoped  $LaMnO_3$  which is an antiferromagnetic insulator containing the typical  $Mn^{3+}$  Jahn-Teller ion with electronic configuration  $t_{2g}^3 e_g^1$  is orbitally double degenerate and is known to undergo such a cooperative Jahn-Teller transition at  $T_{JT} \approx 750$  K. The  $e_g$  orbitals of  $Mn^{3+}$  ions are ordered in the  $a$ - $b$  plane in such a way that at the neighbouring Mn sites, the alternating  $d_{3x^2-r^2}$  and  $d_{3y^2-r^2}$  are occupied in the staggered arrangement shown in Figure 2. The local  $MnO_6$  octahedra are alternatively elongated along the  $x$  and  $y$  directions. The same orbital arrangement is repeated along the  $c$ -axis. This particular orbital ordering (called C-type) presumably induces the A-type antiferromagnetic phase below  $T_N \approx 140$  K in which ferromagnetic  $a$ - $b$  planes are stacked antiferromagnetically along the  $c$ -axis. This relationship of the

orbital and magnetic ordering can be understood from the well-known Goodenough-Kanamori-Anderson rules [7]. According to these rules, the magnitude and the sign of the exchange depend on the type of orbitals that are occupied. If the orbitals are directed towards each other, a strong antiferromagnetic coupling is expected whereas if they are directed away from each other (staggered arrangement or orthogonal to each other), then we have a ferromagnetic interaction.

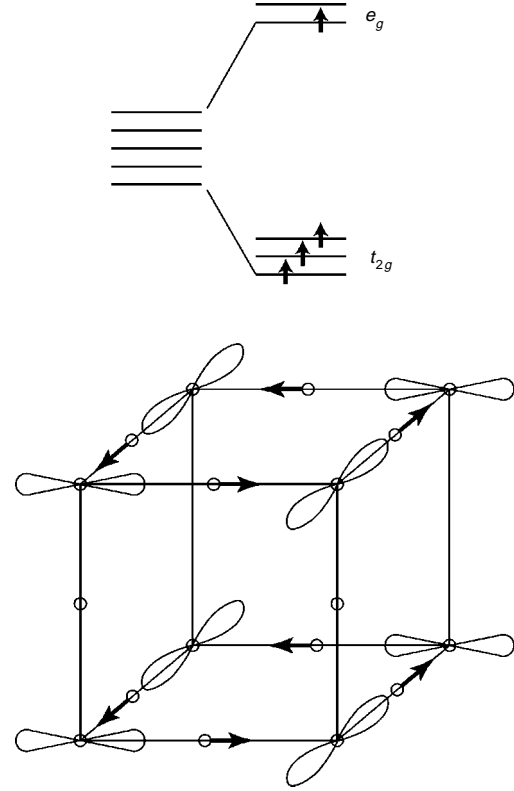


**Figure 2.** Up: Splitting of 3d-levels in a cubic crystal field (regular  $MnO_6$ -octahedron). Electron occupation of the four 3d-electrons in  $Mn^{3+}$  is shown by arrows. Down: Orbital ordering of  $LaMnO_3$ . Arrows indicate the displacements of oxygen ions [from [17]].

Let us now discuss the possible interactions of degenerate orbitals that can lead to orbital ordering. Essentially there exist two such mechanisms in transition metal oxides. The first is the Jahn-Teller interaction of the degenerate orbitals with the lattice distortion [22]. Another possible mechanism was proposed by Kugel and Khomskii [23–25] which is a direct generalisation of the usual superexchange [26] to the case of orbital degeneracy. To describe orbital ordering, it is convenient to introduce operators  $T_i$  of the pseudospin  $\frac{1}{2}$ , describing the orbital occupation, so that the state  $|T^z = \frac{1}{2}\rangle$  corresponds to the occupied orbital  $|3z^2 - r^2\rangle$  and  $|T^z = -\frac{1}{2}\rangle$  corresponds to the occupied orbital  $|x^2 - y^2\rangle$ . The first one corresponds to a local elongation of the  $MnO_6$  octahedra ( $Q_3 > 0$ ) and the second one to a local contraction ( $Q_3 < 0$ ) shown in Figure 3. The second

degenerate  $E_g$  phonon  $Q_2$  which can also lift  $E_g$  degeneracy corresponds to the pseudospin operator  $T^x$ . One can now describe any arbitrary distortion and the corresponding wave function by linear superposition of  $\left|T^z = \frac{1}{2}\right\rangle$  and  $\left|T^z = -\frac{1}{2}\right\rangle$  by

$$|\theta\rangle = \cos\frac{\theta}{2}\left|\frac{1}{2}\right\rangle + \sin\frac{\theta}{2}\left|-\frac{1}{2}\right\rangle, \quad (4)$$

where,  $\theta$  is an angle in the  $(T^z, T^x)$ -plane. This equation is simply a generalisation of the eq. (3) given before.

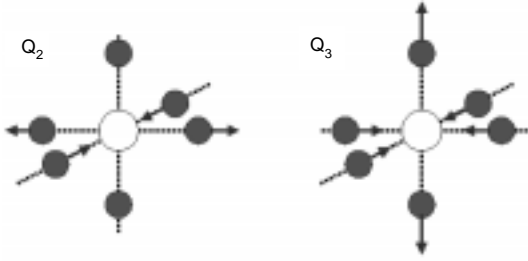


**Figure 3.** Schematic representation of the  $Q_2$  and  $Q_3$  Jahn-Teller modes of a  $\text{MnO}_6$  octahedron [from [17]].

The electron-phonon interaction is the basis of the Jahn-Teller mechanism for orbital ordering and the corresponding Hamiltonian can be written as

$$H = \sum_{iq} g_{iq} \left[ T_i^z (b_{3q}^\dagger + b_{3,-q}) + T_i^x (b_{2q}^\dagger + b_{2,-q}) \right] + \sum_{\alpha q} \omega_{\alpha q} b_{\alpha q}^\dagger b_{\alpha q}, \quad (5)$$

where  $\alpha = 2, 3$  and  $b_3^\dagger$  and  $b_2^\dagger$  are the phonon operators corresponding to the  $Q_3$  and  $Q_2$  local modes. Excluding the phonons by a standard procedure, one obtains the orbital interaction having the form of a pseudospin-pseudospin interaction

$$H_{\text{eff}} = \sum_{ij} J_{ij}^{\mu\nu} T_i^\mu T_j^\nu, \quad (6)$$

where

$$J_{ij} \sim \sum_q \frac{g_q^2}{\omega_q} e^{iq(R_i - R_j)} \quad (7)$$

and  $\mu, \nu = x, z$ . The interaction given by the eq. (6) is in general, anisotropic due to the different dispersion of the different relevant phonon modes, and due to the anisotropic nature of electron-phonon coupling.

The exchange mechanism of orbital ordering may be described by the Hamiltonian containing the pseudospins  $T_i$ , but it contains also the ordinary spins  $S_i$ . The effective superexchange Hamiltonian has the form

$$H = \sum_{ij} \left\{ J_1 S_i S_j + J_2 (T_i T_j) + J_3 (S_i S_j)(T_i T_j) \right\}. \quad (8)$$

The orbital part  $(T_i T_j)$  is in general, anisotropic like (6) but the spin exchange is Heisenberg-like. The exchange mechanism given by (8) describes not only the orbital and spin orderings separately, but also the coupling between them given by the last term. This mechanism is rather successful in explaining the spin and orbital structure in a number of materials [23–25]. The C-type orbital and A-type antiferromagnetic ordering of undoped  $\text{LaMnO}_3$  has been investigated theoretically by several authors by considering the above-mentioned two mechanisms for orbital interactions [27–35].

We will now consider the high temperature structural phase transition in  $\text{LaMnO}_3$  in some detail. The room temperature crystal structure of  $\text{LaMnO}_3$  is orthorhombic (space group  $Pbnm$ ) with lattice parameters  $a = 5.5219$ ,  $b = 5.7312$  and  $c = 7.6731$  Å. The unit cell of this distorted orthorhombic structure is derived from the ideal cubic perovskite structure by choosing two face diagonals and doubling the third axis:  $a = \sqrt{2}a_0$ ,  $b = \sqrt{2}b_0$  and  $c = 2c_0$ . The structure consists of Jahn-Teller distorted  $\text{MnO}_6$  octahedra containing three non-equivalent Mn-O distances, namely short  $s = 1.902$ , medium  $m = 1.963$  and long  $l = 2.172$  Å. Also the Mn-O-Mn bond is no longer straight but has two bond angles  $\theta_1 = 155.5$  and  $\theta_2 = 155.2$  degrees. Figure 4(a) shows a schematic representation of the crystal structure of  $\text{LaMnO}_3$  and Figure 4(b) illustrates schematically the

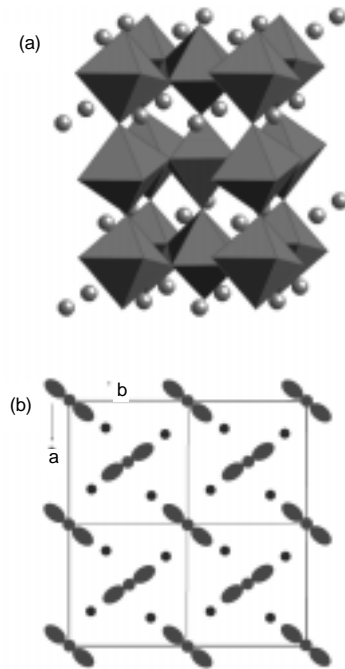


**Figure 4.** (a) Schematic representation of the orthorhombic crystal structure of  $\text{LaMnO}_3$  in which only the La ions and the  $\text{MnO}_6$  octahedra are shown. (b) The staggered ordering of the  $d_{3x^2-r^2}$  and  $d_{3y^2-r^2}$  orbitals in the  $a$ - $b$  plane. The orbital ordering pattern is repeated along the  $c$  axis [from Chatterji *et al.* [39]].

projection of the ordering of the  $d_{3x^2-r^2}$  and  $d_{3y^2-r^2}$  orbitals in the  $a$ - $b$  plane. The orbital ordering pattern is repeated along the  $c$ -axis. The A-type magnetic structure of  $\text{LaMnO}_3$  was determined by Wollan and Koehler [3] by neutron diffraction. The high temperature structural transition at  $T_{JT} \approx 750$  K has been observed in earlier studies [36,37]. The phase transition of  $\text{LaMnO}_3$  has been investigated more recently by Rodriguez-Carvajal *et al* [38] and Chatterji *et al* [39] by both neutron diffraction and high resolution X-ray diffraction with synchrotron radiation. The powder samples were obtained by crushing single crystal ingots. The phase transition is identified to be a Jahn-Teller transition below which the  $e_g$  orbitals become long range ordered. The phase transition has also been investigated by resistivity measurements [41–43]. Figure 5 shows the temperature variation of the resistivity  $\rho$  of undoped  $\text{LaMnO}_3$  along with that of  $\text{La}_{1-x}\text{Ca}_x\text{MnO}_3$  for  $x = 0, 0.025, 0.05, 0.075$  and  $0.10$ . The resistivity  $\rho$  of  $\text{LaMnO}_3$  decreases with increasing temperature and shows a sharp decrease of two orders of magnitude at the JT transition temperature  $T_{JT} \approx 750$  K and the width of the transition is about 2 K. At high temperatures above  $T_{JT}$ ,  $\rho$  is almost temperature independent for  $\text{LaMnO}_3$ . Figure 6 shows the X-ray diffraction diagram of the high

temperature (HT) phase of  $\text{LaMnO}_3$  at  $T = 823$  K. The inset gives parts of the diffraction patterns at several temperatures showing the diffraction peaks of the low temperature (LT) and high temperature (HT or O) phases and their temperature dependence [from Chatterji *et al.* [43]].

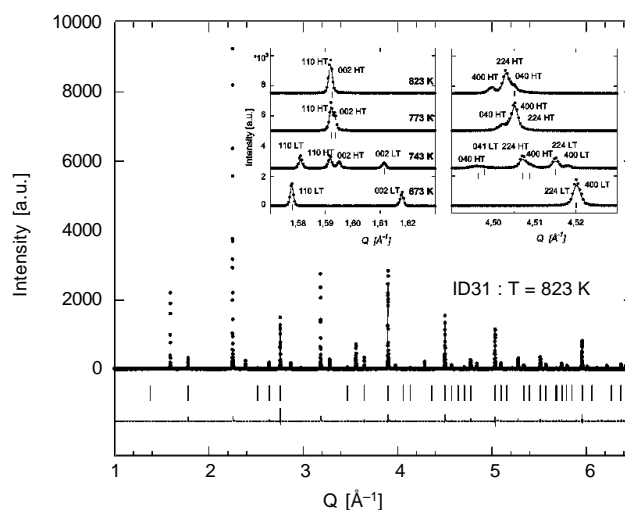


**Figure 6.** X-ray diffraction diagram of  $\text{LaMnO}_3$  at  $T = 823$  K. The inset shows parts of the diffraction patterns at several temperatures showing the diffraction peaks of the low temperature (LT or O') and high temperature (HT or O) phases and their temperature dependence [from Chatterji *et al.* [43]].

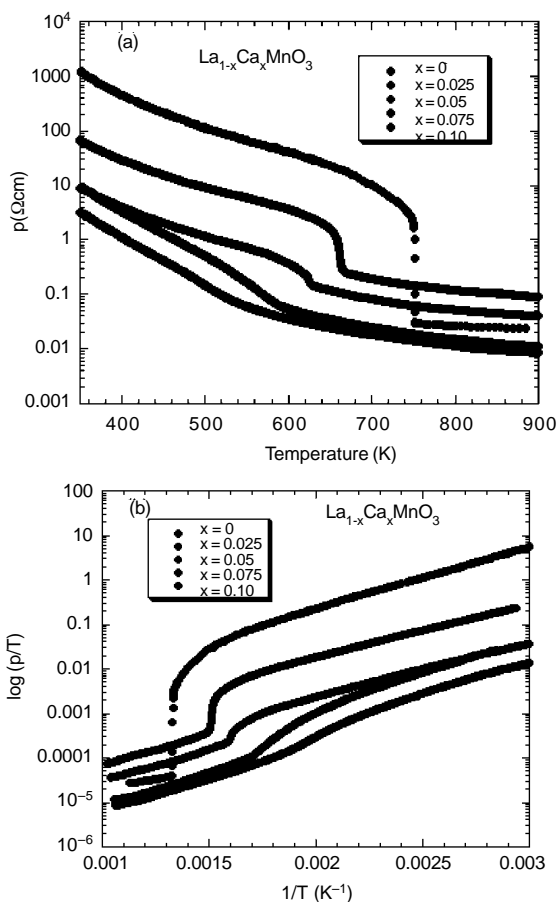


**Figure 5.** (a) Resistivity  $\rho$  of  $\text{La}_{1-x}\text{Ca}_x\text{MnO}_3$  for  $x = 0, 0.025, 0.05, 0.075$  and  $0.10$  as a function of temperature. (b)  $\log_{10}(\rho/T)$  versus  $1/T$  plot of the same data showing linear regions [from Chatterji *et al.* [43]].

high temperature (HT) phases and their temperature dependence. The lattice parameter  $b$  decreases and the parameters  $a$  and  $c/\sqrt{2}$  increase with temperature and then abruptly become almost equal (metrically almost cubic) at  $T_{JT}$ . The transition is clearly first order, because in a temperature range of about 10 K, both the high temperature and low temperature phases coexist. Figure 7 shows the temperature variation of the lattice parameters of  $\text{LaMnO}_3$ . Figure 8(a) shows the temperature variation of the unit cell volume  $V$  of  $\text{LaMnO}_3$ , which increases linearly as a function of temperature from room temperature to about 600 K and deviates from this linear behaviour at higher temperatures. It shows a local maximum at about  $T = 720$  K and then decreases with increasing temperature and finally drops abruptly at

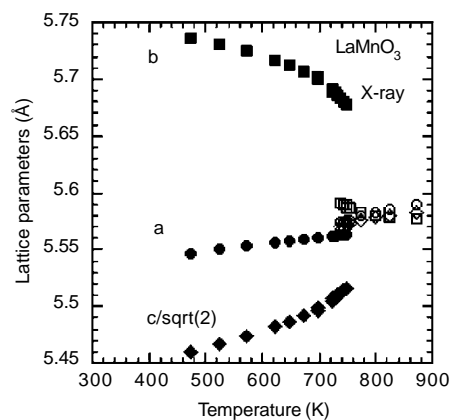


**Figure 7.** Temperature variation of the lattice parameters of  $\text{LaMnO}_3$ . The error bars are smaller than the sizes of the data symbols [from Chatterji *et al.* [39]].

$T_{JT} \approx 750$  K with a volume contraction of about 0.36% at  $T_{JT}$ . At higher temperature,  $V$  increases linearly again with increasing temperature. Figure 8 (b) shows the temperature variation of  $\Delta V$  which is obtained from  $V$  after subtracting the cell volume (“base volume”) obtained by the linear fit of the high temperature data. The temperature variation of this extra volume  $\Delta V$  looks like an order parameter that decreases continuously at first and then drops abruptly to zero (“base volume”) at  $T_{JT}$ .

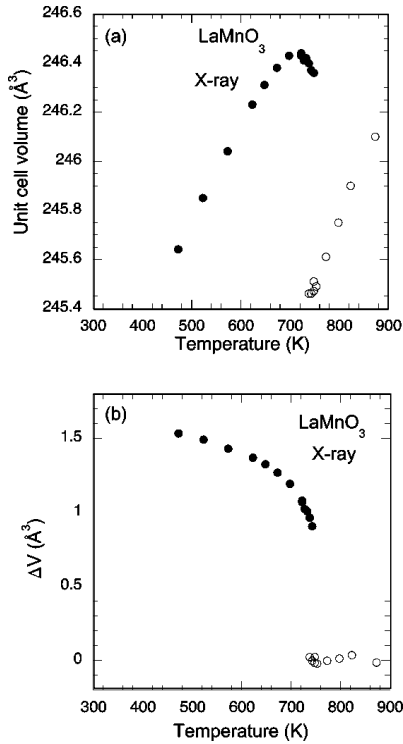


**Figure 8.** (a) Temperature variation of the unit cell volume of  $\text{LaMnO}_3$ . (b) Temperature variation of the unit cell volume after subtraction of the base volume. The error bars are smaller than the sizes of the data symbols [from Chatterji *et al.* [39]].

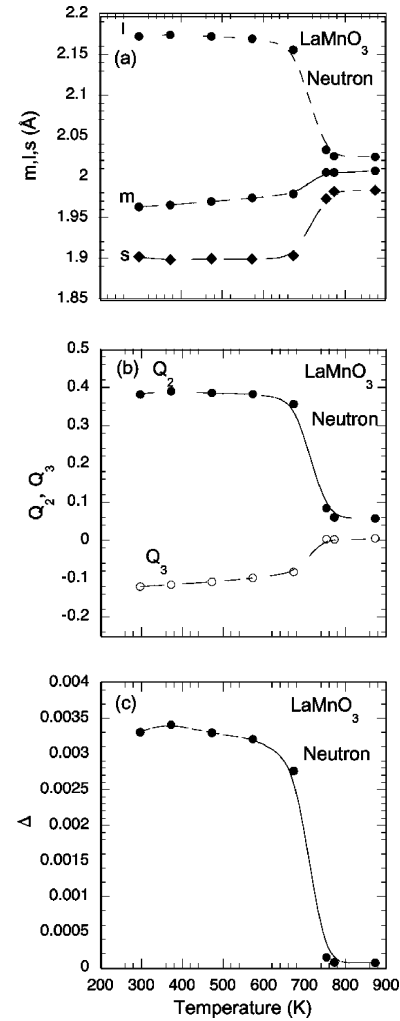
High resolution X-ray diffraction from  $\text{LaMnO}_3$  gave very accurate lattice parameters and unit cell volume. However, X-ray diffraction is not as sensitive as neutron diffraction for determining the positional parameters of O atoms. Chatterji *et al.* [39] performed high temperature neutron powder diffraction measurements at a few selected temperatures to determine positional and thermal parameters of La, Mn and O atoms from Rietveld refinements. The distortion of the  $\text{MnO}_6$  octahedron due to the Jahn-Teller effect produces three Mn-O bond distances: long ( $l$ ), short ( $s$ ) and medium ( $m$ ). The distorted crystal structure can be obtained from the ideal perovskite structure in the following way: first the distortion  $Q_2$  of the octahedron formed with  $\text{O}^{2-}$  ions is added in a staggered way along the three directions, and then the distortion  $Q_3$  is superposed on it. These two distortion modes are expressed in terms of  $l$ ,  $s$ ,  $m$  by

$$Q_2 = \frac{2}{\sqrt{2}}(l-s), \quad Q_3 = \frac{2}{\sqrt{6}}(2m-l-s). \quad (9)$$

The distortion parameter  $\Delta$  of an N-coordination polyhedron  $\text{BO}_N$  with an average B-O distance  $\langle d \rangle$  is defined as

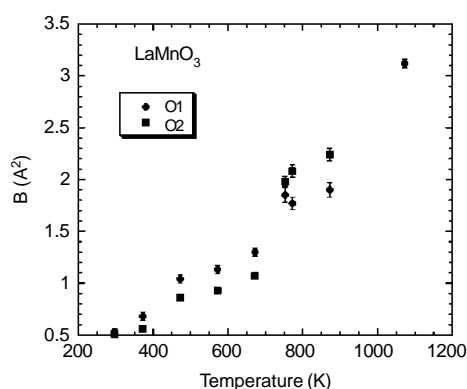
$$\Delta = \frac{1}{N} \sum_{n=1..N} \left\{ \frac{d_n - \langle d \rangle}{\langle d \rangle} \right\}^2. \quad (10)$$

Figure 9(a) shows the temperature dependence of the short  $s$ , long  $l$  and medium  $m$  Mn-O bond distances determined from neutron diffraction data. Figure 9(b) shows the temperature dependence of the two distortion modes  $Q_2$  and  $Q_3$ . Figure 9(c) gives the temperature dependence of the distortion parameter  $\Delta$ . The average Mn-O bond distance  $\langle d \rangle$  shows an abrupt contraction of about 0.45% at  $T_{JT}$ . Thermal parameters of all atoms increase as a function of temperature. However, the thermal parameters of the O atom become very large in the high temperature orthorhombic O and the rhombohedral R phases. Figure 10 shows the temperature variation of the Debye-Waller isotropic temperature factor of the O1 and O2 atoms of  $\text{LaMnO}_3$ .



**Figure 9.** (a) Temperature variation of the three Mn-O bond lengths  $m$ ,  $l$ ,  $s$  of  $\text{LaMnO}_3$ . (b) Temperature variation of the two octahedral distortion modes,  $Q_2$  and  $Q_3$  defined in eq. (1). (c) Temperature variation of the distortion parameter defined in eq. (2). The smoothed curves are guides to the eye [from Chatterji *et al.* [39]].

The isotropic Debye-Waller temperature of the O1 atom increases linearly, but that of O<sub>2</sub> shows an abrupt increase at  $T_{JT} \approx 750$  K.



**Figure 10.** Temperature variation of the Debye-Waller isotropic temperature factor of the O atoms of LaMnO<sub>3</sub>.

The negative thermal expansion in a narrow temperature range and the abrupt volume contraction at  $T_{JT}$  in LaMnO<sub>3</sub> are connected with the orbital order-disorder transition. The orbitally disordered state allows more efficient packing of the MnO<sub>6</sub> octahedra. The situation can be compared with the volume reduction as ice melts into water. The orbitally-ordered state with Jahn-Teller distorted octahedra requires more volume much as do the directionally ordered hydrogen bonds in ice. However, orbital melting is essentially an electronic phenomenon whereas

ice melting is a melting of the crystal. The enthalpy change at the melting of ice [40] is  $\Delta H = 333.5 \text{ J g}^{-1} = 6.008 \text{ kJ mol}^{-1}$  which is about twice that ( $\Delta H = 3.18 \text{ kJ mol}^{-1}$ ) of LaMnO<sub>3</sub> at  $T_{JT}$ . The analogy should not be taken too far. However, it is curious that the temperature variation of the density of LaMnO<sub>3</sub> (Figure 11) shows some qualitative similarity with that of ice, keeping in mind that the volume contraction at  $T_{JT}$  in LaMnO<sub>3</sub> is only 0.36% whereas that at the melting of ice, is about 8%, more than an order of magnitude higher. It is to be noted that the resistivity of LaMnO<sub>3</sub> which decreases with increasing temperature, shows a precursor effect and then drops abruptly at  $T_{JT}$  by more than an order of magnitude [41–43] in a way which mimics the temperature variation of volume (Figure 8). The drop in resistivity indicates that the  $e_g$  electrons become delocalized [44] above  $T_{JT}$ . It is interesting to consider whether electron delocalization is assisted by the volume contraction at  $T_{JT}$  through the modification of the electronic structure.

Let us now discuss the effect of Ca doping on the Jahn-Teller transition in LaMnO<sub>3</sub>. Chatterji *et al.* [43] have investigated the effect of Ca doping on the Jahn-Teller transition in LaMnO<sub>3</sub>, by resistivity and high temperature X-ray diffraction with synchrotron radiation. The resistivity data of La<sub>1-x</sub>Ca<sub>x</sub>MnO<sub>3</sub> at the Jahn-Teller transition were already shown in Figure 5. In general, the resistivity of La<sub>1-x</sub>Ca<sub>x</sub>MnO<sub>3</sub> at a particular temperature  $T$ , decreases with the doping  $x$ . However, this is not always the case. For example, the resistivity of LaMnO<sub>3</sub> is lower than those of La<sub>1-x</sub>Ca<sub>x</sub>MnO<sub>3</sub> with  $x = 0.025$  and  $0.05$  above  $T_{JT}$ . Also the  $\rho(T)$  curves of the two samples for  $x = 0.05$  and  $0.075$  intersect at about  $T = 350$  K. The amount of drop in resistivity at  $T_{JT}$  decreases with increasing  $x$ . The drop in resistivity at  $T_{JT}$  can no longer be seen for the sample  $x = 0.075$  in Figure 5. But the temperature variation of the resistivity shows a change in slope at  $T_{JT}$ . The  $\rho(T)$  for the sample with  $x = 0.10$  also shows only a change in slope at  $T_{JT}$ . The JT transition temperature has been estimated from the  $\rho(T)$  data as  $T_{JT} \approx 750, 660, 620, 580$  and  $540$  K for the samples with  $x = 0, 0.025, 0.050, 0.075$  and  $0.10$ , respectively. At high temperatures above  $T_{JT}$ ,  $\rho$  is almost temperature independent for LaMnO<sub>3</sub>, whereas  $\rho(T)$  exhibits temperature dependence like that for  $T \leq T_{JT}$  for  $x > 0$  samples. In manganites, the formation of small lattice polarons due to strong electron-phonon coupling and their properties in the vicinity of the ferromagnetic transition and beyond have been reported from various measurements [41,45–55]. In the case of small polaronic conduction, the transport mechanism at high temperatures is thermally activated hopping of carriers and the resistivity  $\rho$  can be described well by

$$\rho(T) = \rho_0 \exp(E_\rho/kT) = \frac{akT^n}{g_d e^2 v_0} \exp(E_\rho/kT), \quad (11)$$

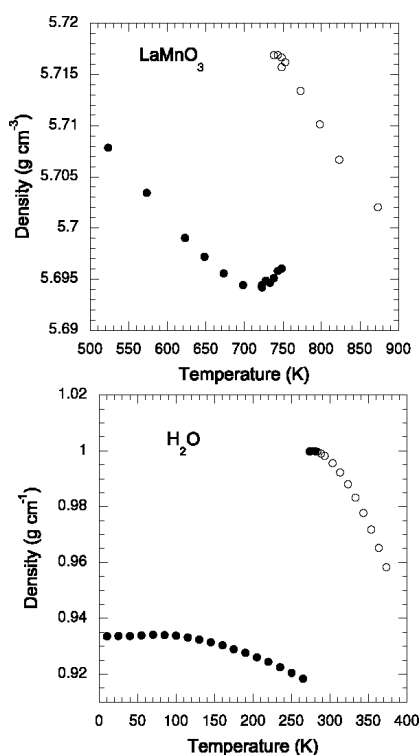


**Figure 11.** (a) Temperature variation of the density of LaMnO<sub>3</sub> close to  $T_{JT}$ . (b) Temperature variation of the density of ice close to the ice melting [from Chatterji *et al.* [39]].

where  $a$  is the jump distance of the polaron,  $E_\rho$  is the activation energy of the polaron,  $\nu_0$  is the characteristic phonon frequency of the system and  $g_d$  is a constant that depends on the lattice structure. For the adiabatic hopping of polarons,  $n = 1$ , and for the nonadiabatic case,  $n = 3/2$ . Although  $\rho$  decreases monotonically with increasing doping concentration, the activation energy  $E_\rho$  obtained from the slope of the  $\log_{10}(\rho/T)$  versus  $1/T$  plot shown in Figure 5(b), is almost independent of Ca concentration up to  $x = 0.10$ . The present measurements of the temperature dependence of resistivity of  $\text{La}_{1-x}\text{Ca}_x\text{MnO}_3$  show clearly that the resistivity is a highly sensitive function of the orbital order. The details of the fit of the resistivity data with the small polaron hopping model are given by Mandal *et al* [41].

The powder samples of  $\text{La}_{1-x}\text{Ca}_x\text{MnO}_3$  were obtained by crushing single-crystal ingots. High temperature X-ray powder diffraction experiments were done on the high resolution powder diffractometer at the undulator beam line ID31 of the European Synchrotron Radiation Facility in Grenoble. The X-ray wavelength was  $0.50183 \pm 0.00005 \text{ \AA}$ . Figure 12 shows a part of the diffraction diagram of  $\text{La}_{1-x}\text{Ca}_x\text{MnO}_3$  for  $x = 0.025$  at several temperatures close to  $T_{JT}$ . The figure illustrates the temperature evolution of 110 and 001 peaks of the low temperature (LT or O') and high temperature (HT or O) phases close to the Jahn-

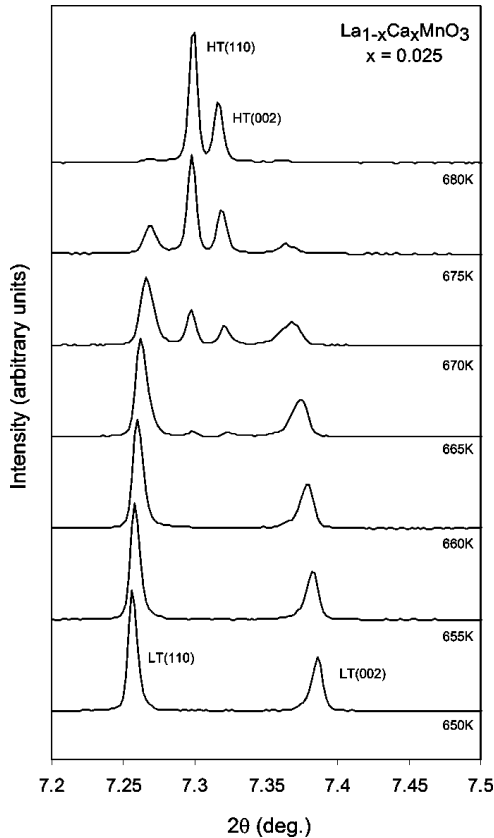


**Figure 12.** X-ray diffraction diagram of  $\text{La}_{1-x}\text{Ca}_x\text{MnO}_3$  for  $x = 0.025$  at several temperatures close to  $T_{JT}$  showing the diffraction peaks of the low temperature (LT or O') and high temperature (HT or O) phases and their temperature dependence.

Teller transition. We note that the peaks corresponding to the high and low temperature phases coexist in a temperature range of at least 10 K. To illustrate how the Jahn-Teller transition evolves with doping, we show in Figure 13 also a part of the

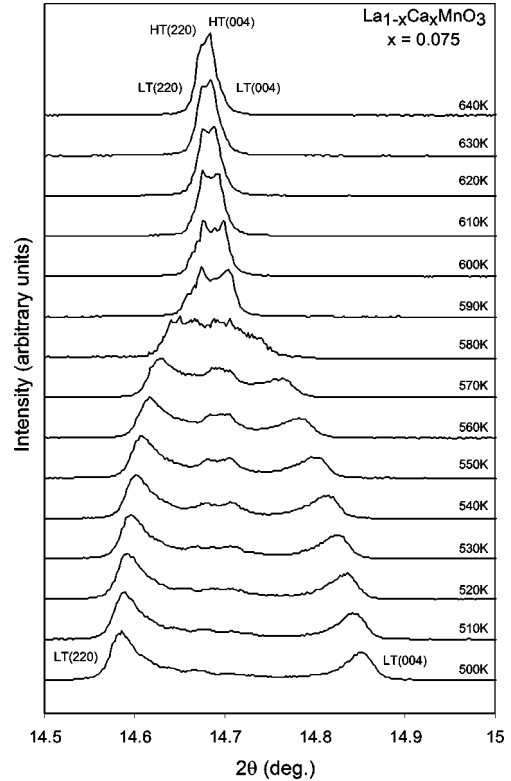


**Figure 13.** X-ray diffraction diagram of  $\text{La}_{1-x}\text{Ca}_x\text{MnO}_3$  for  $x = 0.075$  at several temperatures close to  $T_{JT}$  showing the diffraction peaks of the low temperature (LT or O') and high temperature (HT or O) phases and their temperature dependence.

diffraction diagram of  $\text{La}_{1-x}\text{Ca}_x\text{MnO}_3$  for  $x = 0.075$  at several temperatures close to  $T_{JT}$ . Here, we choose to illustrate the temperature evolution of 220 and 004 peaks of the low

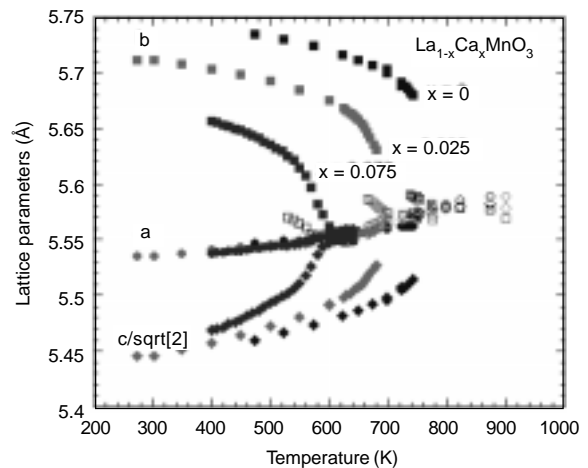


**Figure 14.** Temperature variation of the lattice parameters of  $\text{La}_{1-x}\text{Ca}_x\text{MnO}_3$  for  $x = 0, 0.025$  and  $0.075$ . The error bars are smaller than the sizes of the data symbols. The filled and open symbols correspond to the low temperature O' and high temperature O phases, respectively [from Chatterji *et al.* [43]].

temperature (LT or O') and high temperature (HT or O) phases close to the Jahn-Teller transition. The range in temperature for which the two phases coexist is much wider in this case. Also the transition is more continuous. The Rietveld analysis of the complete diffraction diagrams yielded the lattice parameters as a function of temperature plotted in Figure 14. We note that the lattice parameter  $b$  decreases continuously with temperature and then contracts abruptly at  $T_{JT}$  whereas  $c/\sqrt{2}$  increases continuously and expands abruptly at  $T_{JT}$ . The unit cell parameter  $a$  increases very slowly with temperature and can be considered almost temperature independent. The above behaviour is similar for the sample with  $x = 0$  and 0.025 although the amount of discontinuity at  $T_{JT}$  decreases for the doped sample. For the sample with  $x = 0.075$ , the lattice parameters change continuously with temperature and show no abrupt

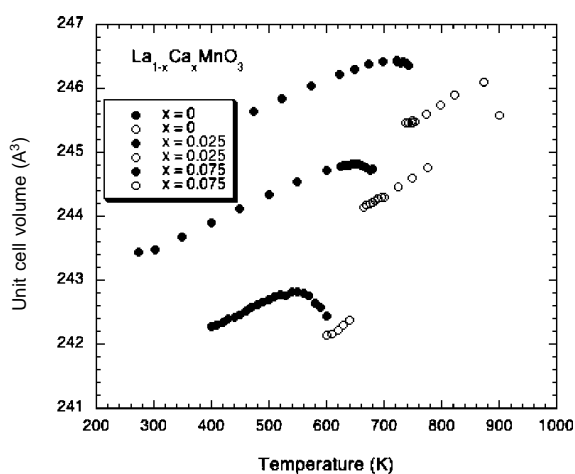


**Figure 15.** Temperature variation of the unit cell volume of  $\text{La}_{1-x}\text{Ca}_x\text{MnO}_3$  for  $x = 0, 0.025$  and  $0.075$ . The filled and open symbols correspond to the low temperature O' and high temperature O phases, respectively [from Chatterji *et al.* [43]].

change at the phase transition temperature. Figure 15 shows the temperature dependence of the unit cell volume of  $\text{La}_{1-x}\text{Ca}_x\text{MnO}_3$  for  $x = 0, 0.025$  and  $0.075$ . The unit cell volume of undoped  $\text{LaMnO}_3$  increases linearly and after showing a local maximum, decreases and then undergoes an abrupt volume contraction of 0.36 % at  $T_{JT}$ . Above the phase transition temperature, the unit cell volume increases again linearly with temperature. The doped sample with  $x = 0.025$  behaves in a similar way but the amount of volume contraction at  $T_{JT}$  is reduced substantially. The sample with  $x = 0.075$  shows little or no volume contraction at  $T_{JT}$  and the volume can be considered to decrease continuously and then increase with increasing temperature. Figure 16 shows the temperature variation of  $\Delta V$  which is obtained from  $V$  after subtracting the unit cell volume ("base volume") obtained by the linear fit of the high temperature data. The temperature variation of this extra volume  $\Delta V$  looks like an order parameter of the phase transition which decreases continuously at first and then drops abruptly to zero ("base volume") at  $T_{JT}$ . Also the amount of volume contraction

decreases with doping  $x$ . Thus, temperature dependence of both the lattice parameters and the unit cell volume indicates a

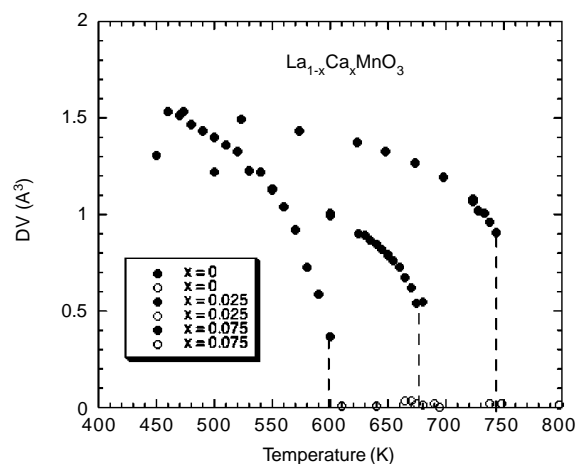


**Figure 16.** Temperature variation of the excess unit cell volume  $\Delta V$  of  $\text{La}_{1-x}\text{Ca}_x\text{MnO}_3$  for  $x = 0, 0.025$  and  $0.075$  after subtraction of the base volume as explained in the text. The filled and open symbols correspond to the low temperature O' and high temperature O phases, respectively. The determination of the "base volume" of  $\text{La}_{1-x}\text{Ca}_x\text{MnO}_3$  for 0.075 was uncertain due insufficient high temperature data and therefore the excess unit cell volume  $\Delta V$  could not be determined very accurately [from Chatterji *et al.* [43]].

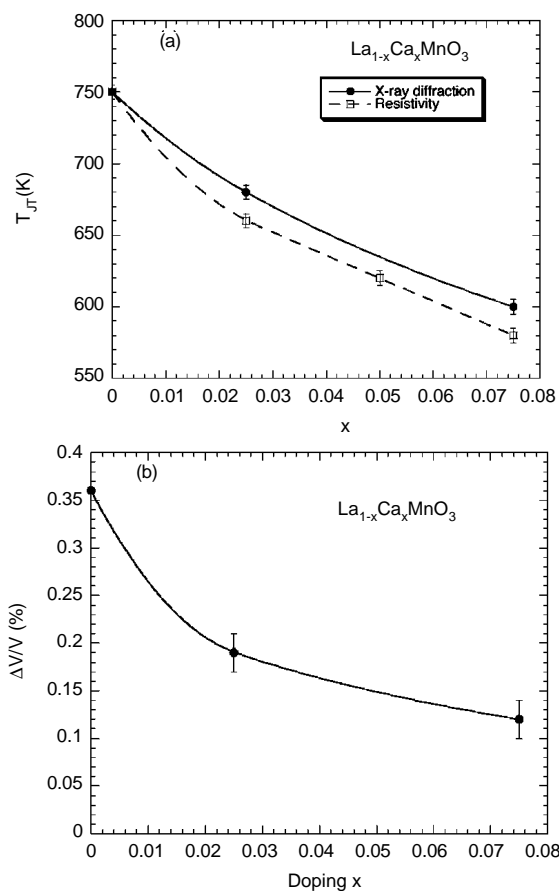


**Figure 17.** Doping dependence of (a) the Jahn-Teller transition temperature  $T_{JT}$  and (b) the volume contraction  $\Delta V/V$  at the transition. The continuous curves are only guides to the eye.

crossover from a discontinuous to the continuous behaviour across  $T_{JT}$ . The critical doping level  $x_c$  is perhaps somewhat greater than 0.075. We have not investigated  $\text{La}_{1-x}\text{Ca}_x\text{MnO}_3$  for  $x > 0.075$  by X-ray diffraction but we did resistivity measurements for samples up to the doping level  $x = 0.125$ . The indication of crossover behaviour was already obtained earlier [17] in  $\text{La}_{1-x}\text{Ba}_x\text{MnO}_3$ . However, the temperature interval in this investigation was not fine enough to make any definite conclusion. The Jahn-Teller transition temperatures for  $\text{La}_{1-x}\text{Ca}_x\text{MnO}_3$  are about 750, 680 and 600 for  $x = 0, 0.025$  and  $0.075$ , respectively. The volume contractions at  $T_{JT}$  for  $\text{La}_{1-x}\text{Ca}_x\text{MnO}_3$  are about 0.36%, 0.19%, and 0.12% for  $x = 0, 0.025$  and  $0.075$ , respectively. The hole doping thus decreases both the transition temperature and the volume contraction and tends to make the transition continuous. Figure 17 shows the doping dependence of the Jahn-Teller transition temperature  $T_{JT}$  and the volume contraction  $\Delta V/V$  of  $\text{La}_{1-x}\text{Ca}_x\text{MnO}_3$  at the transition.

The Rietveld analysis of conventional X-ray and neutron powder diffraction data uses the information on the position and intensities of the Bragg peaks. The diffuse scattering also recorded in the diffraction diagrams is treated as background and is neglected. Further, the fitting of the intensity data is usually done with a well ordered crystalline model obeying the space group symmetry. Such analysis therefore gives information at best about the time and space averaged structure. In recent years, an alternative method of analysing diffraction data has been developed [56], which uses information buried in between the Bragg peaks in the form of diffuse scattering, in addition to the Bragg peaks. It is the method of pair-distribution function (PDF) analysis imported from research on glasses and liquids. This method can reveal structure on the local scale and is similar to that of EXAFS in this respect. The conventional structural analysis using Bragg intensities described above suggests that the Jahn-Teller distortion of the  $\text{MnO}_6$  octahedra is removed above the phase transition. However, the investigations with local probes like EXAFS and PDF analysis [57,58] seem to suggest that the Jahn-Teller distorted octahedra in  $\text{LaMnO}_3$  remain distorted both below and above the phase transition. The analysis of the pair-distribution function (PDF) obtained from the neutron data reveals [58] that the distortion implied by the unequal Mn-O bond distances, remains unchanged on the local scale of about 16 Å. The authors suggest that 16 Å nano-clusters of short-range orbital order persist in the high temperature O and R phases. It is necessary to reconcile this picture with the abrupt resistivity drop [41,44] at  $T_{JT}$  and its near temperature independent behaviour above  $T_{JT}$ . The drop of resistivity at  $T_{JT}$  is not expected in going from the ordered to the disordered phase. One would naively expect an increase in the resistivity in the disordered phase due to the increased scattering of the charge carriers. It is likely that the dynamic nature of the Jahn-Teller distortion is connected with the

resistivity drop at the phase transition. Also the volume contraction at  $T_{JT}$  may cause a change in the electronic structure by changing the electron bandwidth and thereby leading to a change in the electron-phonon coupling. The modified electron-phonon coupling constant can lead to a drastic change [59] in the temperature variation of resistivity which is known to be of polaronic character in  $\text{LaMnO}_3$ .

Chatterji *et al* [39] intuitively argued that the volume contraction in pure  $\text{LaMnO}_3$  is due to a more efficient packing of the  $\text{MnO}_6$  octahedra in the orbitally disordered or liquid state. Maitra *et al* [60] have studied the volume collapse of  $\text{LaMnO}_3$  at the Jahn-Teller (JT) transition temperature based on a model Hamiltonian involving pseudo-spin of  $\text{Mn}^{3+} e_g$  states, the staggered JT distortion and the volume strain coordinate. The anharmonic coupling between these primary and secondary order parameters lead to the first-order JT phase transition associated with a comparatively large volume reduction  $\Delta V/V \approx 10^{-2}$ . A continuous change to a second-order transition as a function of the anharmonic coupling parameter was obtained if this parameter is reduced from the value appropriate for pure  $\text{LaMnO}_3$ . So the crossover behaviour as a function of Ca doping found in the present investigation is consistent with that obtained theoretically by Maitra *et al* [60]. However, this is a phenomenological theory and therefore does not explain how Ca doping reduces the anharmonic coupling parameter.

The remarkable similarity between the volume contraction shown in Figure 8 and the resistivity drop shown in Figure 5 at  $T_{JT}$  strongly indicates that the transport in  $\text{LaMnO}_3$  is directly coupled to the order parameter of the phase transition. We argue that at the Jahn-Teller transition, the localised  $e_g$  electrons become more delocalized. The samples are still insulators and the conduction is still consistent with the polaron hopping model. However, the phonon-electron coupling strength [60] is changed at the transition, making the slopes of the temperature dependence of resistivity much lower at temperatures above  $T_{JT}$ . The true mechanism of electron delocalization in a single-valent  $\text{LaMnO}_3$  consisting only of  $\text{Mn}^{3+}$  above  $T_{JT}$  however remains unclear.

It is to be noted that the orbital liquid O phase is the phase which supports the CMR effect. This phase can be produced either by heating or by doping with holes. There seem to exist three strict conditions for generating CMR effect: (1) the orbital long range order must be destroyed, (2) the phase should approach a cubic symmetry and (3) one must have enough doped holes to produce a ferromagnetic ground state and an insulator-to-metal transition at a temperature close to  $T_C$ . The conditions (1) and (2) are of course related because the destruction of long range orbital order reduces the orthorhombicity of the lattice and makes it closer to cubic. We suggest that understanding the microscopic mechanism of the Jahn-Teller phase transition

in  $\text{LaMnO}_3$  and its dependence on hole doping, is crucial to understanding the CMR effect. In conclusion, we may add that the connection between the resistivity anomaly and the volume contraction that has been established by the work described above, will certainly impose severe constraints on any microscopic theory of the Jahn-Teller transition in  $\text{LaMnO}_3$ .

### Acknowledgments

I thank B Ouladdiaf, F Fauth, B Ghosh and P Mandal for collaboration and T Ziman for critical discussions and also for suggesting the phrase 'orbital ice'. I wish to thank S Mason for reading the manuscript very carefully and suggesting improvements.

### References

- [1] J G Bednorz and K A Müller *Z. Phys.* **B64** 189 (1986)
- [2] G H Jonker and J H V Santen *Physica* **16** 337 (1950)
- [3] E O Wollan and W C Koehler *Phys. Rev.* **100** 545 (1955)
- [4] C Zener *Phys. Rev.* **82** 403 (1951)
- [5] P W Anderson and H Hasegawa *Phys. Rev.* **100** 67 (1955)
- [6] P-G de Gennes *Phys. Rev.* **118** 141 (1960)
- [7] J B Goodenough *Magnetism and the Chemical Bond* (New York : John Wiley) (1963)
- [8] R M Kusters, D A Singleton, D A Keen, R McGreevy and W Hayes *Physica* **B155** 362 (1989)
- [9] K Chabara, T Ohno, M Kasai and Y Kozono *Appl. Phys. Lett.* **63** 1990 (1993)
- [10] R von Helmolt, J Wocker, B Holzapfel, L Schultz and K Samwer, *Phys. Rev. Lett.* **71** 2331 (1993)
- [11] S Jin, T H Tiefel, M McCormack, R A Fastnacht, R Ramesh and L H Chen *Science* **264** 413 (1994)
- [12] Y Tokura, A Urushibara, Y Moritomo, T Arima, S Asamitsu, G Kido and N Furukawa *J. Phys. Soc. Jpn.*, 3931 (1994)
- [13] A Asamitsu, Y Moritomo, Y Tomioka, T Arima and Y Tokura *Nature* (London) **373** 407 (1995)
- [14] Y Tokura and N Nagaosa *Science* **288** 462 (2000)
- [15] K I Kugel and D I Khomskii *Sov. Phys. JETP* **52** 501 (1981)
- [16] A J Millis, P B Littlewood and B I Shraiman *Phys. Rev. Lett.* **74** 5144 (1995)
- [17] For more recent works see for example *Colossal Magnetoresistive Manganites* (ed.) T Chatterji, (Amsterdam : Kluwer Academic) (2004) and the references therein.
- [18] Y Tokura (ed.) *Colossal Magnetoresistive Oxides* (Amsterdam : Gordon and Breach) (2000)
- [19] G Herzberg *Atomic Spectra and Atomic Structure* (Engelwood Cliffs, N J : Prentice Hall) (1937)
- [20] L Pauling and E B Wilson *Introduction to Quantum Mechanics* (New York : McGraw-Hill) (1935)
- [21] H A Jahn and E Teller *Proc. Roy. Soc. London Ser. A* **161** 220 (1937)
- [22] G A Gehring and K A Gehring *Rep. Prog. Phys.* **38** 1 (1975)
- [23] K I Kugel and D Khomskii *JETP Lett.* **15** 446 (1972)
- [24] K I Kugel and D Khomskii *Sov. Phys. -JETP Lett.* **37** 725 (1973)
- [25] K I Kugel and D Khomskii *Sov. Phys. Usp.* **25** 231 (1982)
- [26] P W Anderson *Phys. Rev.* **115** 2 (1959)
- [27] J Kanamori *J. Appl. Phys.* **31** 14S (1960)
- [28] M Kataoka and J Kanamori *J. Phys. Soc. Jpn.* **32** 113 (1972)
- [29] A J Millis *Phys. Rev.* **B53** 8434 (1996)
- [30] M Kataoka *J. Phys. Soc. Jpn.* **70** 2353 (2001)
- [31] N Nagaosa, S Murakami and H C Lee *Phys. Rev.* **B57** R6767 (1998)
- [32] L F Feiner and A M Oleś *Phys. Rev.* **B59** 9923 (1999)
- [33] P Benedetti and R Zeyher *Phys. Rev.* **B59** 9923 (1999)
- [34] J Bala and A M Oleś *Phys. Rev.* **B62** R6085 (2000)
- [35] S Okamoto, S Ishihara and S Maekawa *Phys. Rev.* **B65** 144403 (2002)
- [36] A Wold and R Arnott *J. Phys. Chem. Solids* **9** 176 (1959)
- [37] G H Jonker *et al.*, *J. Appl. Phys.* **37** 1424 (1966)
- [38] J Rodriguez-Carvajal, M Hennion, F Moussa and A H Moudden *Phys. Rev.* **B57** R3189 (1998)
- [39] T Chatterji, F Fauth, B Ouladdiaf, P Mandal and B Ghosh *Phys. Rev.* **B68** 052406 (2003)
- [40] see for example, R A Alberty and R J Silbey *Physical Chemistry* (2nd edn) (New York : Wiley) (1996)
- [41] P Mandal, B Bandyapadhyay and B Ghosh *Phys. Rev.* **B64** R180405 (2001)
- [42] T Chatterji, B Ouladdiaf, P Mandal and B Ghosh *Solid State Commun.* **131** 75 (2004)
- [43] T Chatterji, D Reily, P Mandal and B Ghosh *Phys. Rev.* **B73** 094444 (2006)
- [44] J-S Zhou and J B Goodenough *Phys. Rev.* **B60** R15002 (1999)
- [45] T Holstein *Ann. Phys. (N.Y.)* **8** 343 (1959)
- [46] J Yamashita and T Kurosawa *J. Phys. Chem. Solids* **5** 34 (1958)
- [47] J Yamashita and T Kurosawa *J. Phys. Soc. Jpn.* **15** 802 (1960)
- [48] For a review on polarons, see for example *J. Appl. Solid State Phys.* (eds) F Seitz, D Turnbull and H Ehrenreich **vol.21** p.193 (New York : Academic) (1968)
- [49] S J L Billinge, R G DiFrancesco, G H Kwei, J J Neumeier and J D Thompson *Phys. Rev. Lett.* **77** 715 (1996)
- [50] P Dai, J A Fernandez-Baca, N Wakabayashi, E W Plummer, Y Tomioka and Y Tokura *Phys. Rev. Lett.* **85** 2553 (2000)
- [51] X J Chen, S Soltan, H Zhang and H-U Habermeier *Phys. Rev.* **B65** 174402 (2002)
- [52] G Y Snyder, M R Beasley and T H Geballe *J. Appl. Lett.* **69** 4254 (1996)
- [53] L Wang, J Yin, S Huang, X Huang, J Xu, Z Liu and K Chen *Phys. Rev.* **B60** R6976 (1999)
- [54] M Jaime, M B Salamon, M Rubinstein, R E Treece, J S Horwitz and D B Chrisey *Phys. Rev.* **B54** 11914 (1996)
- [55] M Jaime, H T Hardner, M B Salamon, M Rubinstein, P Dorsey and D Emin *Phys. Rev. Lett.* **78** 951 (1997)
- [56] T Egami and S J L Billinge *Underneath the Bragg Peaks* (Amsterdam : Pergamon) (2003)
- [57] M C Sánchez, G Subías, J García and J Blasco *Phys. Rev. Lett.* **90** 045503 (2003)
- [58] X Qiu, T Proffen, J F Mitchell and S J L Billinge *Phys. Rev. Lett.* **94** 177203 (2005)
- [59] S Fratini and S Ciuchi *Phys. Rev. Lett.* **91** 256403 (2003)
- [60] T Maitra, P Thalmeier and T Chatterji *Phys. Rev.* **B69** 132417 (2004)